Assessing Effects of Permafrost Thaw on C fluxes based on a Multi-Year Modeling across a Permafrost Thaw Gradient at Stordalen, Sweden

Jia Deng[1], Changsheng Li[1], Steve Frolking[1], Yu Zhang[2], Kristina Bäckstrand[3], Patrick Crill[3]

[1]Earth Systems Research Center, Institute for the Study of Earth, Oceans and Space, University of New Hampshire, 39 College Road, Durham, NH 03824, USA

[2]Canada Centre for Mapping and Earth Observation, Natural Resources Canada, 588 Booth Street, Ottawa, ON K1A 0Y7, Canada

[3]Department of Geological Sciences, Stockholm University, 106 91 Stockholm, Sweden

*Corresponding author: Changsheng Li

Tel.: +1603 862 1771

Email: cs_li_98@yahoo.com

Keywords: Permafrost thaw, Peatlands, NEE, CH_4 flux, DNDC

Abstract

Northern peatlands in permafrost regions contain a large amount of organic carbon (C) in the soil. Climate warming and associated permafrost degradation are expected to have significant impacts on the C balance of these ecosystems, but the magnitude is uncertain. We incorporated a permafrost model, Northern Ecosystem Soil Temperature (NEST), into a biogeochemical model, DeNitrification-DeComposition (DNDC), to model C dynamics in high-latitude peatland ecosystems. The enhanced model was applied to assess effects of permafrost thaw on C fluxes of a sub-arctic peatland at Stordalen, Sweden. DNDC simulated soil freeze/thaw dynamics, net ecosystem exchange of CO_2 (NEE), and CH_4 fluxes across three typical land cover types, which represent a gradient in the process of ongoing permafrost thaw at Stordalen. Model results were compared with multi-year field measurements and the validation indicates that DNDC was able to simulate observed differences in seasonal soil thaw, NEE, and CH_4 fluxes across the three land cover types. Consistent with the results from field studies, the modeled C fluxes across the permafrost thaw gradient demonstrate that permafrost thaw and the associated changes in soil hydrology and vegetation increase net uptake of C from the atmosphere, but also increase the annual to decadal radiative forcing impacts on climate due to increased CH_4 emissions. This study indicates the potential of utilizing biogeochemical models, such as DNDC, to predict soil thermal regime in permafrost areas and to investigate impacts of permafrost thaw on ecosystem C fluxes after incorporating a permafrost component into the model framework.

1 Introduction

Northern peatlands are characterized by cold and wet conditions that promote the accumulation of soil organic carbon (SOC) (e.g., Johansson T.et al., 2006; Schuur et al., 2008). These ecosystems have accumulated 473-621 Pg (10^{15} g) carbon (C) since the Last Glacial Maximum (Yu et al., 2010), with more than 277 Pg C stored in permafrost areas (Schuur et al., 2008; Tarnocai et al., 2009). Although northern peatlands generally acted as sinks of carbon dioxide (CO_2) in the past and under current climate (e.g., Lund et al., 2010; McGuire et al., 2009); peat C stocks may be released to the atmosphere with climate warming, due to mobilization of previously frozen C in permafrost soils and accelerated decomposition of SOC (e.g., Frolking et al., 2011; McGuire et al., 2009; Schuur et al., 2009, 2011). In addition, because of prevailing anaerobic soil conditions, northern peatlands are an important source of atmospheric methane (CH_4), releasing 31-65 Tg $CH_4\,yr^{-1}$ (McGuire et al., 2009) and methane emissions can change with permafrost thaw (Christensen et al., 2004).

Pronounced warming has been observed in northern high latitudes, with surface air temperature increased by approximately 0.09˚C $decade^{-1}$ during the 20^{th} century (ACIA, 2005). More pronounced warming has been projected in this region for the 21^{st} century (IPCC, 2007). As a result of climate warming, degradation of permafrost has been documented in northern peatlands (e.g., James et al., 2013; Payette et al., 2004; Quinton et al., 2011; Åkermanand Johansson, 2008). Permafrost thaw can result in increases in active layer thickness (ALT; the thickness of surface soil layer that freezes and thaws seasonally above a year-round frozen layer) and cause land surface subsidence, which in turn may cause changes in topography, soil hydrology, and vegetation (e.g., Avis et al., 2011; Johansson M. et al., 2006; Schuur et al., 2008).

These changes associated with permafrost degradation can significantly affect the C cycle in northern ecosystems (e.g., Dorrepaal et al., 2009; Johansson T. et al., 2006; McGuire et al., 2009; Schneider von Diemling et al., 2012).

Although much concern has been placed on the C balance in permafrost ecosystems, large uncertainty still exists (e.g., Koven et al., 2011; McGuire et al., 2009; Schuur et al., 2011). Northern peatlands are highly heterogeneous, usually with varying characteristics of permafrost, topography, hydrology, soil, and vegetation within close proximity (Nungesser, 2003), which results in considerable variations of C fluxes at local and landscape scales (e.g., Bäckstrand et al., 2010; Lund et al., 2010; Sachs et al., 2010). Responses of the C balance to permafrost degradation have been shown to vary across different peatlands as well (Bäckstrand et al., 2010). Therefore, it is an ongoing challenge to extrapolate site-specific measurements to large regions.

Process-based models are effective tools to assess the impacts of climate change on boreal ecosystems. Several large-scale models have been enhanced by incorporating thermal, hydrologic, vegetation, and biogeochemical processes in relation to permafrost conditions and these models have been applied to quantify the impacts of climate change on C fluxes at regional and global scales (e.g., Schneider von Diemling et al., 2012; Wania et al., 2009a, 2009b; Zhuang et al., 2001, 2004, 2006). Predictions by large-scale models are generally done at coarse spatial resolutions, therefore disregarding the effects of local spatial heterogeneity. By ignoring fine-scale spatial heterogeneity in vegetation and environmental conditions, systematic biases may occur in simulations of permafrost degradation and C fluxes (Bohn and Lettenmaier, 2010; Zhang et al., 2013). In addition, the results based on coarse-scale

91 modeling are difficult to validate by comparing with field observations and
92 uncertainty may arise in regional and global simulations due to limited validation
93 (Kirschke et al., 2013).
94
95 A process-based biogeochemical model, DeNitrification-DeComposition (DNDC),
96 was recently enhanced by incorporating a permafrost model, Northern Ecosystem
97 Soil Temperature (NEST), for predicting biogeochemistry in high latitudes from plant
98 communities to ecosystem scale. The model was initially tested against one growing
99 season of CH_4 flux data measured at a permafrost site in the Lena River Delta, Russia
100 (Zhang et al., 2012). In this study, we applied the enhanced model to assess effects of
101 permafrost thaw on C fluxes of a well-studied sub-arctic peatland at Stordalen,
102 Sweden. The study peatland is located in a discontinuous permafrost zone and
103 consists of palsas – small, relatively dry plateaus elevated one to a few meters due to
104 subsurface ice lenses (Williams and Smith, 1989) – and intervening low, wetter areas.
105 These palsas can expand and shrink in extent with relatively small variations in
106 environmental conditions such as temperatures or winter snow packs (Payette et al.
107 2004), and represent one class of permafrost (Davis, 2001). Stordalen's palsas are
108 extremely vulnerable to changing climate and widespread degradation of permafrost
109 is expected to occur (Åkerman and Johansson, 2008). DNDC simulated multi-year
110 soil freeze/thaw dynamics, net ecosystem exchange of CO_2 (NEE), and CH_4 fluxes
111 across three typical land cover types, which represent a gradient of permafrost
112 degradation in the study region. During simulations, different soil hydrologic
113 conditions and vegetation characteristics of these land cover types were used as
114 model inputs, therefore we focused on predicting the changes in soil thermal
115 dynamics and C cycling along with thawing. The model was tested against long-term

field measurements to verify its applicability for simulating the differences in soil thermal regime and C fluxes across a gradient of permafrost thaw. Then we assessed the possible impacts of permafrost thaw on C fluxes for the Stordalen peatland based on the multi-year simulations. A validated simulation model provides a mechanism for not only interpreting observations but also predicting the impacts of future climate change on greenhouse gas emissions.

2 Methods and data

2.1 The study area and field observations

The study area is the Stordalen mire (68˚20’N, 19˚03’E, 351 ma.s.l.) located 10 km southeast of Abisko Scientific Research Station (ANS) in northern Sweden. It is a sub-arctic peatland with discontinuous permafrost. This area has a continental climate, with an annual mean air temperature of 0.07 ˚C and an average annual precipitation of 308 mm during 1986-2006 according to the observations at ANS (Callaghan et al., 2010). Long-term climate records at ANS indicate that the annual mean air temperature in this region has increased by 2.5 °C from 1913 to 2006, significantly exceeding the 0 °C threshold for the first time during the last few decades (Bäckstrand et al., 2008; Callaghan et al., 2010). This warming has led to a thicker active layer and permafrost disappearance in this area (Åkerman and Johansson, 2008). The degradation of permafrost has significantly affected surface topography, hydrology, and vegetation, and thereby exerted a strong influence on the fluxes of CO_2 and CH_4 (Christensen et al., 2004; Johansson T. et al., 2006; Malmer et al., 2005; Åkerman and Johansson, 2008).

As in most peatlands in permafrost regions, Stordalen mire has high spatial

heterogeneity in topography (1-2 m relative differences in elevation). The topographic variability creates small-scale (meters) environments with different soil moisture and nutrient conditions that support different plant communities (Rosswall et al., 1975; Bäckstrand et al., 2008). The area can be broadly classified into three typical land cover types (i.e., dry Palsa, semi-wet Sphagnum, and wet Eriophorum; note that in this study the terms Sphagnum and Eriophorum indicate land cover types instead of vegetation species). The Palsa sites of Stordalen are dry features underlain by permafrost, with an ALT usually < 0.7 m in late summer; the Sphagnum sites are also underlain by permafrost, representing intermediate thaw features, with an ALT generally thicker than 1.0 m in late summer, and are wetter than the Palsa with water table levels fluctuate close to the ground surface; the Eriophorum sites have no permafrost and are generally wetter than Sphagnum, with water table levels constantly near or above the ground surface (Bäckstrand et al., 2008, 2010; Olefeldt and Roulet, 2012). Therefore these three land cover types have different permafrost regimes and soil water conditions, which support different vegetation compositions (Bäckstrand et al., 2008, 2010). During the last three decades, there have been pronounced shifts in the extent of these three land cover types, with Palsa being converted into Sphagnum or Eriophorum dominated land cover (Christensen et al., 2004; Malmer et al., 2005). These three land cover types can be regarded as representing a gradient of permafrost degradation (e.g., Malmer et al., 2005; Johansson T. et al., 2006; Bäckstrand et al., 2010).

CO_2 and CH_4 fluxes were measured using automated chambers at Stordalen during 2003 to 2009. NEE was measured at three sites (i.e., the Palsa, Sphagnum, and Eriophorum sites) to represent three typical land cover types, and CH_4 emissions were

consistently observed at the Sphagnum and Eriophorum sites, where water table levels were above or near the peat surface (Bäckstrand et al., 2008, 2010). The Palsa site is relatively dry and its CH_4 flux is near zero (Bäckstrand et al., 2008). For each plot, an auto-chamber system measured CO_2 and total hydrocarbon (THC) fluxes every three hours and there were eight measurements per day. CH_4 fluxes were manually observed approximately three times per week by taking samples from every chamber and these measurements were used to quantify the proportion of CH_4 in the measured THC (Bäckstrand et al., 2008, 2010). Daily NEE and CH_4 fluxes were calculated as average values of eight measurements. During 2003 to 2009, valid rates of daily NEE were calculated for 85-213 days in a year based on the field measurements. Daily CH_4 fluxes were available for 79-116 days in a year, with an exception in 2006 when the instrument was down (Bäckstrand et al., 2008, 2010). In addition, soil thaw depth (measured to 90 cm) and water table depth (WTD) were measured 3-5 times per week from early May to mid October each year (Bäckstrand et al., 2008). Daily meteorological data, including air temperature, precipitation, solar radiation, wind speed, as well as relative humidity, were recorded at the ANS (Figure 1). The technical details regarding the measurements of NEE and CH_4 fluxes, and the relevant auxiliary variables were described by Bäckstrand et al. (2008, 2010).

2.2Modification of DNDC

2.2.1 Overview of the DNDC model

DNDC is a process-based model developed for quantifying C sequestration as well as the emissions of carbon and nitrogen (N) gases from terrestrial ecosystems (Li et al., 1992a, 1992b, 2000; Stange et al., 2000; Zhang et al., 2002). The model has incorporated a relatively complete suite of biophysical and biogeochemical processes,

which enables it to compute the complex transport and transformations of C and N in terrestrial ecosystems under both aerobic and anaerobic conditions.

DNDC is comprised of six interacting sub-models: soil climate, plant growth, decomposition, nitrification, denitrification, and fermentation. The soil climate, plant growth, and decomposition sub-models convert the primary drivers, such as climate, soil properties, vegetation, and anthropogenic activity, into soil environmental factors, such as soil temperature and moisture, pH, redox potential (Eh), and substrate concentrations. The nitrification, denitrification, and fermentation sub-models simulate C and N transformations that are mediated by soil microbes and controlled by soil environmental factors (Li, 2000; Li et al., 2012). In DNDC, NEE is calculated as the difference between net primary production (NPP) and soil microbial heterotrophic respiration (HR). NPP is simulated at daily time step by considering the effects of several environmental factors on plant growth, including radiation, air temperature, soil moisture, and N availability. The model simulates the production of plant litter and incorporates the plant litter into pools of soil organic matter (SOM). HR is calculated by simulating decomposition of SOM. SOM is divided into four pools in DNDC, namely litter, microbes, humads, and passive humus. Each pool is further divided into two or three sub-pools with specific C to N (C/N) ratios and decomposition rates. As a microbially-mediated process, decomposition of each SOM fraction depends on its specific decomposition rate as well as soil thermal and moisture conditions (Li et al., 2012). Methane flux is predicted by modeling CH_4 production, oxidation, and transport processes. CH_4 production is simulated by calculating substrate concentrations (i.e., electron donors and acceptors) resulting from decomposition of SOC as well as plant root activities including exudation and

respiration, and then by tracking a series of reductive reactions between electron donors (i.e., H_2 and dissolved organic carbon) and acceptors (i.e., NO_3^-, Mn^{4+}, Fe^{3+}, SO_4^{2-}, and CO_2). In DNDC, CH_4 production and oxidation can occur simultaneously within a soil layer but within relatively aerobic and anaerobic micro-sites, whose volumetric fractions are defined by an Eh calculator, a so-called “anaerobic balloon”, embedded in the model framework (Li, 2007). Redox potential, temperature, pH, along with the concentrations of electron donors and acceptors are the major factors controlling the rates of CH_4 production and oxidation. CH_4 is transported from soil into atmosphere via plant-mediated transport, ebullition, and diffusion (Fumoto et al., 2008; Zhang et al., 2002).

2.2.2 Soil freeze/thaw and permafrost dynamics

Traditionally, DNDC simulated soil thermal dynamics by a relatively simple module without detailed processes describing the soil thermal regime in the presence of permafrost. It did not explicitly simulate energy exchange within soil-vegetation-atmosphere system, snowpack thermal dynamics, the presence of permafrost, or active layer dynamics (Zhang et al., 2002). However, these processes or environmental factors are important for characterizing the permafrost regime, soil thermal dynamics, soil hydrology, or C and N cycles in high latitudes (e.g., Riseborough et al., 2008; Waelbroeck, 1993). In order to make DNDC more suitable for northern ecosystems, especially frozen soil conditions, we incorporated a permafrost model, NEST, into the model framework (Zhang et al., 2012). NEST is a process-based model which simulates ground thermal dynamics, soil freeze/thaw dynamics, and permafrost conditions (Zhang et al., 2003). In NEST, soil temperature and permafrost thermal regime are calculated by solving the heat conduction equation,

241 with the upper boundary condition determined by surface energy balance and the
242 lower boundary condition being defined as the geothermal heat flux. The effects of
243 climate, vegetation, snow pack, ground features, and hydrological conditions on the
244 soil thermal regime are incorporated into the model on the basis of energy and water
245 exchanges within soil-vegetation-atmosphere system (Zhang et al., 2003, 2005). To
246 ensure that DNDC simulates permafrost environmental factors and biogeochemistry
247 in synchrony, NEST's functions, which describe soil thermal and hydrologic regimes,
248 were embedded into the framework of DNDC at the model code level. After coupling
249 to NEST, DNDC was able to simulate both the seasonal dynamics of active layer and
250 the long-term variations of permafrost as well as their impacts on biogeochemical
251 processes (Zhang et al., 2012). Therefore, the model should better serve
252 investigations of impacts of climate change on C fluxes in high-latitude ecosystems.
253
254 **2.3 Model application**
255 We performed DNDC simulations for the three typical Stordalen land cover types
256 (Palsa, Sphagnum, and Eriophorum) from 2002 to 2009. Daily meteorological data
257 (i.e., maximum, mean, and minimum air temperature, precipitation, solar radiation,
258 wind speed, and humidity) from 2002 to 2009 recorded at the ANS were collected to
259 support the simulations. All sites had a surface soil layer of peat (0.5 m) overlying a
260 silt soil layer (Rosswallet al., 1975; Rydeńet al., 1980; Olefeldtet al., 2012). The peat
261 had a bulk density of 0.15 g cm^{-3}, SOC content of 0.5 kg C kg^{-1} SDW (soil dry
262 weight), total porosity of 0.9, field capacity of 0.4 (water-filled pore space), wilting
263 point of 0.15 (water-filled pore space), and pH (H_2O) of 5.0, according to
264 observations from Malmer and Walleń (1996), Rydeń et al. (1980), and Öquist and
265 Svensson (2002). The local bedrock is granite (Rosswallet al., 1975) and a thermal

conductivity of 2.9 W m^{-1} $°C^{-1}$ was used (Clauser and Huenges, 1995). The geothermal heat flux in the study region was estimated as 0.06 W m^{-2} (Majorowiczet al., 2011).

While the three land cover types share common conditions regarding weather, geology, and soil during the simulations, they differ in soil hydrologic conditions and vegetation characteristics. In order to predict the dynamics of water table at the Sphagnum and Eriophorum sites, DNDC used several parameters to estimate lateral flows, including surface inflow rate, maximum water table depths for surface and ground outflows, as well as surface and ground outflow rates (Zhang et al., 2002). We estimated these parameters by comparing the modeled and observed WTD (Table 1). To reduce the influence of WTD prediction-error on soil thermal and biogeochemical processes, the observed WTDs were used during the simulations if the measurements were available, and the simulated WTDs from this calibrated model were used to interpolate daily values between observations. WTD observations at the Sphagnum and Eriophorum sites were made on about one-third of the days across seven growing seasons from 2003 to 2009. For the Palsa site, we assumed that there is no surface lateral inflow and water will flow away each day when the water table is above the land surface or water infiltrates into frost table, based on local studies (Rydeń et al., 1980). DNDC also requires phenological and physiological parameters to simulate plant growth, including maximum biomass production and its partitioning to shoot and root, vegetation C/N ratio, required thermal degree days for vegetation growth, plant water requirement, and an index of biological N fixation. These parameters for the three land cover types were determined either based on literature or as model defaults (Table 2).

To initialize the soil climate conditions, the soil thermal and hydrological modules of DNDC were iteratively run by using the climate data in 2002 until the simulated annual mean soil temperature was stable. Then the vegetation and soil biogeochemical modules were activated and the model was run continuously from 2002 to 2009. (Note that soil initial conditions have only a small influence on DNDC output as compared to other factors, therefore, although we did not turn on the vegetation and soil biogeochemical modules during the initialization of soil climate conditions, potential errors in soil initial conditions due to this were small.) We validated the model by using the measured soil thaw depth, NEE, and CH_4 fluxes; using the sign convention that positive values represent net CO_2 or CH_4 emissions into the atmosphere and negative fluxes represent net CO_2 or CH_4 uptake. Two statistical indexes, the relative root mean squared error (RRMSE, equation 1) and the coefficient of correlation (R, equation 2), were used to quantity the accordance and correlation between model predictions and field observations (Moriasi et al., 2007).

$$RRMSE = \frac{100}{\overline{|o|}} \sqrt{\frac{\sum_{i=1}^{n} (p_i - o_i)^2}{n}} \qquad (1)$$

$$R = \frac{\sum_{i=1}^{n} (o_i - \overline{o})(p_i - \overline{p})}{\sqrt{\sum_{i=1}^{n} (o_i - \overline{o})^2 \sum_{i=1}^{n} (p_i - \overline{p})^2}} \qquad (2)$$

In both equations, o_i and p_i are the observed and simulated values, respectively; $\overline{o}$ and $\overline{p}$ are their averages; and n is the number of values. In addition, we decomposed the root mean squared error into systematic and unsystematic components by using the ordinary least square (OLS) method (Willmott, 1982; Willmott et al., 1985). The systematic and unsystematic root mean squared errors ($RMSE_S$ and $RMSE_U$) were

calculated with equations 3 and 4, respectively:

$$RMSE_S = \sqrt{\frac{\sum_{i=1}^{n}(\widehat{p_i} - o_i)^2}{n}} \quad (3)$$

$$RMSE_U = \sqrt{\frac{\sum_{i=1}^{n}(p_i - \widehat{p_i})^2}{n}} \quad (4)$$

In both equations, $\widehat{p_i}$ is an OLS estimate of p_i and is derived from the regression of p_i on o_i by using the ordinary least square method (Willmott, 1982; Willmott et al., 1985).

To quantify the differences of C fluxes for the three land cover types across the permafrost thaw gradient, we analyzed the simulated annual NEE and CH_4 fluxes from 2003 to 2009. The CH_4 fluxes from dry Palsa were assumed to be zero (Bäckstrand et al., 2008). We calculated net emissions of greenhouse gases (GHG) for the three land cover types as CO_2-equivalents by using a 100-year global warming potential (GWP) of 25 kg CO_2-equivalents kg^{-1} CH_4 (IPCC, 2007). In addition, we estimated the possible impacts of permafrost thaw on C fluxes and GHG emissions for the Stordalen mire based on the model results and changes in the fractions of the three land cover types from 1970 to 2000.

3 Results and analyses

3.1 Model validation

3.1.1 Thaw depth

Figure 2 shows the seasonal dynamics of the observed and simulated thaw depth during 2003 to 2009. As field observations demonstrate, thaw rates varied across the

three land cover types. At the Palsa site, the maximum thaw depth usually ranged from 45 to 60 cm during the summer seasons from 2003 to 2009, while the soil was often thawed to greater than 90 cm (i.e., below the maximum depth of observations) by August or September at the Sphagnum site and by June or July at the Eriophorum sites. Therefore, the thaw rates were relatively slow, moderate, and rapid at the Palsa, Sphagnum, and Eriophorum sites, respectively. In comparison with the observations, the DNDC model generally captured the differences of thaw depth across the three land cover types as well as their seasonal dynamics (Figure 2). The simulations showed that the dry Palsa site had an active layer thickness of around 55 cm. The thaw depth reached deeper than 100 cm by the end of July to September at the semi-wet Sphagnum site and by June or July at the wet Eriophorum site.

The model results demonstrated that rate of summer thaw accelerated along the gradient of soil moisture. Because water-filled pores have higher thermal conductivity than air-filled pores, DNDC simulated the low, moderate, and high values of thermal conductivity at the dry Palsa, semi-wet Sphagnum, and wet Eriophorum sites, respectively, which consequently resulted in the slow, moderate, and fast rates of summer thaw at these three sites. This explanation is consistent with the conclusion based on the local field study (Rydén and Kostov, 1980). However, a few discrepancies remained between the modeled and observed results, primarily in the soil thaw dynamics at the Sphagnum site, where DNDC overestimated the thaw rate during the late periods of soil thaw in most years (Figure 2h to n). Nevertheless, the comparisons between the simulations and observations indicated that DNDC can reliably predict differences in the dynamics of soil thaw at the three land cover types at Stordalen, which is crucial for correctly simulating the impacts of permafrost thaw

on soil hydrology, plant growth, and biogeochemical processes.

3.1.2 NEE

Figure 3a-g illustrates the observed and simulated daily NEE at the Palsa site. The daily observations were highly variable and showed a clear seasonal cycle across 2003 to 2009, with net CO_2 uptake increasing in early summer, CO_2 uptake most days during mid-summer and net CO_2 emissions in late summer and autumn. In comparison with the measurements, DNDC generally captured the magnitude and seasonal characteristics of daily NEE, although discrepancies existed. The R values were calculated for each year and ranged from 0.40 to 0.69 (Figure 3a-g), indicating that there were significant correlations between the simulated and observed daily NEE in each year ($P < 0.0001$). Table 3 lists the observations and simulations on the cumulative NEE for the seven growing periods from 2003 to 2009. The observed cumulative NEE ranged from -435 to -241 kg CO_2-C ha^{-1} and the modeled values ranged from -414 to -265 kg CO_2-C ha^{-1}. The calculated RRMSE values varied between 3% and 25% (mean: 13%) across the seven growing seasons and the discrepancies between the simulations and observations were less than the standard deviations of the observed cumulative NEE in each year (Table 3). These results indicate that DNDC successfully simulated the cumulative NEE during growing seasons.

At the Sphagnum site, the simulated and observed seasonal variations of daily NEE were similar across 2004 to 2009. Both the simulations and observations showed that net CO_2 uptake increased in early summer, prevailed most days during mid-summer, and decreased to net CO_2 emissions in late summer and autumn (Figure 3i-n). The similar patterns suggest that the DNDC model generally captured the seasonal

fluctuations of daily NEE over 2004 to 2009, although discrepancies existed in each year. However, it seems systematic biases appeared in 2003. For example, the field observations showed high net uptake rates of CO_2 during 25 May to 22 June in 2003; while the model predicted lower rates (Figure 3h), primarily because of limitations of low solar radiation, air temperature (the mean was 6.0 ˚C during 25 May to 22 June), and soil temperature on plant productivity. Nonetheless, the modeled and observed daily NEE were significantly correlated in all years ($P < 0.001$ in 2003 and $P < 0.0001$ in other years), and R values ranged from 0.32 to 0.78 (Figure 3h-n). The predicted cumulative NEE ranged from -521 to -203 kg CO_2-C ha^{-1} over seven growing seasons. The results are consistent with the corresponding observations, which ranged from -525 to -212 kg CO_2-C ha^{-1} (Table 3), with the discrepancies between the simulations and observations close to or less than the standard deviations of the observed cumulative NEE in each year. The values of RRMSE ranged from 1% to 17% with a mean of 6% over 2003 to 2009 (Table 3).

At the Eriophorum site, both the simulated and observed daily NEE showed similar seasonal patterns across the studied years, excepting 2004 (Figure 3o-u), with net CO_2 uptake increasing in early summer, CO_2 uptake most days during mid-summer and net CO_2 emissions in late summer and autumn. The R values ranged from 0.39 to 0.74, which indicates significant ($P < 0.0001$) correlations between the modeled and measured daily NEE in each year during 2003 to 2009. However, we also note systematic deviation between the simulations and measurements in 2004. In this year, the field observations showed persistent low net uptake rates of CO_2 during late May to the end of June; while the model predicted an increasing trend of net CO_2 uptake (Figure 3p), because of increasing solar radiation, air temperature, soil temperature,

and soil thaw depth. At the Eriophorum site, the observed daily uptake rates of CO_2 were usually higher than that at the Palsa and Sphagnum sites during summer (Figure 3). The DNDC model captured the differences across these three sites and the magnitudes of the simulated NEE were comparable with the corresponding observations. The simulations of growing season cumulative NEE ranged from -1078 to -365 kg CO_2-C ha^{-1} during 2003 to 2009, which were close to the observations (ranged from -1118 to -270 kg CO_2-C ha^{-1}). The RRMSE values ranged from 1% to 35% (mean: 15%) over 2003 to 2009 (Table 3). The discrepancies between the simulated and observed cumulative NEE were less than the standard deviations of the observations in each year from 2003 to 2007, which indicates DNDC reliably simulated the growing season cumulative NEE over these years. However, the discrepancies were larger than the standard deviations of the observed cumulative NEE in 2008 and 2009 (-571 vs. -471 ± 76 kg C ha^{-1} in 2008, and -365 vs. -270 ± 59 kg C ha^{-1} in 2009), suggesting that the model may have overestimated the CO_2 uptake during growing season in these two years.

3.1.3 Water table and CH_4 fluxes

As shown in Figure 4a-g, WTDs (with positive values for above-ground and negative values for below-ground) fluctuated between -30 to 0 cm at the Sphagnum site, while were generally near or above the ground surface at the Eriophorum site.

Figure 4h-n compares the observed and simulated daily CH_4 fluxes at the Sphagnum site. As illustrated by Figure 4h-n, the simulated seasonal patterns of daily CH_4 fluxes were close to the observations during the six studied years from 2003 to 2009 (excluding 2006, which had no data), with the highest peak appeared in August or

September in both the simulations and field measurements. In addition, DNDC simulated small spikes of CH_4 emission a few days after snowmelt and during post-growing season, which also agreed with the observations (Figure 4l-n). The simulated early CH_4 flux spikes were induced by snowmelt and thaw of surface soil layer, which created water saturation in surface peat and thereby supported CH_4 production and emission. The high fluxes predicted during post-growing season occurred during occasional thaw of the surface soil layer during the early freezing stage, which provided pathways of releasing for both newly produced methane and methane accumulated in the soil profile. The R values ranged between 0.63 and 0.89 over the six years (Figure 4h-n), which indicates the simulated seasonal variation of daily CH_4 fluxes was significantly correlated with the observed seasonal variation in each year ($P < 0.0001$). The similar patterns and significant correlations between the simulated and observed daily CH_4 fluxes suggest that DNDC generally captured the observed seasonal characteristics of CH_4 fluxes, despite a few remaining inconsistencies. The modeled results indicated that the temporal patterns of CH_4 fluxes were primarily controlled by soil temperature and the changes of WTD at the Sphagnum site. Simulated daily CH_4 fluxes were positively correlated with soil temperature ($P < 0.0001$) when WTDs were closer to the peat surface than -10 cm (Figure 5a). Simulated daily CH_4 fluxes were also positively correlated with the WTDs ($P < 0.0001$) if the mean of peat layer (0-50 cm) temperature was higher than 2.0 °C (Figure 5b). Of the six tested sampling periods, the simulated cumulative CH_4 fluxes varied from 12.7 to 35.7 kg CH_4-C ha^{-1}, comparable with the observations, which varied from 9.7 to 30.6 kg CH_4-C ha^{-1} (Table 4). The values of RRMSE ranged from 4% to 35% with a mean of 21% (Table 4). The comparison demonstrates that the discrepancies between the simulated and observed cumulative CH_4 fluxes were close

460 to or less than the standard deviations of the observations in each year.

461

462 At the Eriophorum site, the observed CH_4 fluxes usually started to increase early in
463 the growing season, with high peaks appeared during July to September. Then the
464 CH_4 fluxes decreased during the rest of growing season (Figure 4o-u). The simulated
465 seasonal patterns of daily CH_4 fluxes were comparable with the observations, with a
466 generally increasing trend from the early growing season until mid-summer in each
467 year, when the fluxes reached relatively high levels. Then the simulated CH_4 fluxes
468 started to decrease (Figure 4o-u). The correlations between the modeled and
469 measured daily CH_4 fluxes were statistically significant ($P < 0.0001$) in each year,
470 with R values ranging from 0.47 to 0.89 over the six years. These results suggest that
471 DNDC approximately matched the observed daily CH_4 fluxes over the six studied
472 years from 2003 to 2009 (excluding 2006), although discrepancies existed in each
473 year. However, it seems systematic biases existed in 2008. DNDC underestimated the
474 magnitudes of CH_4 fluxes in 2008 and had a relatively later onset of emissions than
475 observations (Figure 4t). The modeled results demonstrated that the temporal patterns
476 of CH_4 fluxes at the Eriophorum site were mainly related to the changes in soil
477 temperature and the associated variations of plant growth and soil decomposition,
478 because of the inundated conditions at this site, which generated constantly wet
479 anaerobic conditions suitable for CH_4 production. Simulated daily CH_4 fluxes were
480 positively correlated with soil temperature (Figure 5c, $P < 0.0001$), and we did not
481 find any correlation between the simulations of daily CH_4 fluxes and WTD (Figure
482 5d). This conclusion is consistent with the field results (e.g., Bäckstrand et al., 2008;
483 Jackowicz-Korczyński et al., 2010). As illustrated by Figure 4h-u, the observed daily
484 CH_4 fluxes at the Eriophorum site were generally higher than that at the Sphagnum

site. DNDC captured the differences between these two sites. Of the six tested sampling periods, the observed cumulative CH_4 fluxes ranged from 57.9 to 121 kg CH_4-C ha^{-1}, while the modeled results varied from 45.5 to 113 kg CH_4-C ha^{-1}. The RRMSE values ranged from 3% to 22% with a mean of 12% across these six periods (Table 4). The discrepancies between the simulations and observations were close to or less than the standard deviations of the observed cumulative CH_4 fluxes over the studied years excepting 2003 and 2008, which indicates a good accordance between the simulations and observations of CH_4 fluxes over these years. However, the discrepancy was larger than the standard deviation of the observed cumulative CH_4 fluxes in 2003 and 2008 (76.4 vs. 91.8 ± 10.5 kg C ha^{-1} in 2003, and 45.3 vs. 57.9 ± 4.42 kg C ha^{-1} in 2008), suggesting that the model may have underestimated the cumulative CH_4 fluxes in these two years.

3.2AnnualC fluxes and net greenhouse gas emissions

In this section, we review simulated annual (not growing season) NEE and CH_4 fluxes at the Palsa, Sphagnum, and Eriophorum sites from 2003 to 2009. The simulated annual total NEE varied from -132 to +56.5 (Palsa; mean: -50.9), -492 to -191 (Sphagnum; mean: -342), and -1021 to -399 (Eriophorum; mean: -793) kg CO_2-C ha^{-1} yr^{-1}, and inter-annual variability of NEE increased with increasing magnitude (Figure 6a). The predictions of annual total NEE were different across the Palsa, Sphagnum, and Eriophorum sites and primarily resulted from differences in environment conditions, including soil temperature, thaw regime (Figure 2), soil moisture content (Figure 4a-g), and vegetation characteristics (as indicated by the different physiological parameters used for simulating plant growth, Table 2). DNDC predicted the highest uptake rates of CO_2 at the Eriophorum site, primarily due to (1)

the highest value of the maximum productivity under optimum growing conditions (Table 2); (2) the fastest soil thaw rate (Figure 2), which was favorable for water and nitrogen uptake; and (3) a permanently high water table (Figure 4a-g) which restricted soil heterotrophic respiration and provided abundant water for plant transpiration. The lowest rates of annual total NEE were simulated at the Palsa site, primarily because of (1) the lowest value of the maximum productivity under optimum growing conditions (Table 2), (2) the slowest soil thaw rate and limited summer thaw depths (Figure 2), and (3) a relatively dry soil which restricted plant transpiration and was comparatively favorable for soil decomposition.

During 2003 to 2009, the simulations of annual total CH_4 fluxes ranged from 17.9 to 42.2 (Sphagnum; mean: 32.8) and 72.2 to 125 (Eriophorum; mean: 104) kg CH_4-C ha^{-1} yr^{-1}. As with NEE simulations, inter-annual variability of CH_4 fluxes increased with increasing annual means (Figure 6a). The annual total CH_4 fluxes were different across the Sphagnum and Eriophorum sites (Figure 6a). Simulated CH_4 fluxes were higher at the Eriophorum site than the Sphagnum site due to: (1) increased rates of CH_4 production due to higher soil temperature and faster thaw rate, (2) a higher water table that supported CH_4 production while restricting CH_4 oxidation, (3) higher plant growth rates and consequently more substrates (e.g., CO_2 and dissolved organic carbon) used for CH_4 production, and (4) accelerated rates of CH_4 transport due to increased plant vascularity.

Annual net C fluxes were calculated as the sum of annual total NEE and CH_4 fluxes in this study (i.e., horizontal loss of dissolved organic carbon was not considered). Because the CH_4 component was assumed to be zero at the Palsa site, the simulated

annual net C fluxes were equal to annual NEE (range: -132 to 56.5 kg C ha^{-1}, mean: -50.9 kg C ha^{-1}) at this site. Simulations of annual net C fluxes ranged between -462 to -163 (mean: -309) and -934 to -488 (mean: -689) kg C ha^{-1} at the Sphagnum and Eriophorum sites, respectively, during 2003 to 2009. These results illustrated that C uptake rates increased along the permafrost thaw gradient at Stordalen (Figure 6b). Net GHG emissions, expressed as CO_2-equivalents, were calculated by considering more powerful radiative forcing potential of CH_4 than CO_2 (25 times over a 100-year horizon). The simulated annual GHG at the Palsa site varied from -485 to 207 kg CO_2-eq. ha^{-1} yr^{-1}, with a mean of -186 kg CO_2-eq. ha^{-1} yr^{-1} from 2003 to 2009. At the Sphagnum and Eriophorum sites, the annual GHG ranged from -806 to 377 and -849 to 1905 kg CO_2-eq. ha^{-1} yr^{-1}, respectively, and the corresponding means were -162 and 562 kg CO_2-eq. ha^{-1} yr^{-1}, respectively. Therefore, the modeled results demonstrated that for the wetter Eriophorum site, higher CH_4 emissions offset its larger net C sink, and the Palsa site was a larger net sink of CO_2-equivalents than the Eriophorum site (Figure 6b).

3.3 Possible changes of C fluxes due to permafrost thaw at Stordalen

Interpretation of aerial images of Stordalen showed that the area of ‘hummock’ (Palsa) cover declined from 9.2 to 8.3 ha, while the area of ‘semiwet’ and ‘wet’ (Sphagnum) cover increased from 6.0 to 6.2 ha, and ‘tall graminoid’ (Eriophorum) cover increased from 1.3 to 2.0 ha from 1970 to 2000 (Malmer et al., 2005; Johansson T. et al., 2006). These changes in vegetation cover indicate a trend toward a wetter ecosystem probably as a direct consequence of permafrost thaw at Stordalen. Given that soil thaw rate accelerated under wet conditions (Figure 2), this trend toward a wetter ecosystem may further accelerate permafrost degradation. By applying the modeled

annual CO_2 and CH_4 fluxes to these changes in vegetation cover areas, we estimated an increase of 578 kg C yr^{-1} (or 35 kg C ha^{-1} yr^{-1} for the study area of 16.5 ha) in CO_2 uptake and an increase of 79 kg C yr^{-1} (or 4.8 kg C ha^{-1} yr^{-1}) in CH_4 emission from 1970 to 2000 at Stordalen. Using a 100-year GWP value for methane, the net impact due to the vegetation change is a net CO_2 equivalent emission of 527 kg CO_2-eq. yr^{-1}; i.e., the warming impact of increased CH_4 emission more than offsets the cooling impact of increased CO_2 uptake at the mire. If these fluxes from vegetation cover areas (1970 vs. 2000) were to persist for one to two centuries, an analysis with a simple model of atmospheric perturbation radiative forcing (Frolking et al. 2006) shows that the different atmospheric lifetimes of CO_2 and CH_4 are such that the CO_2 sink would overcome the CH_4 emissions in terms of instantaneous radiative forcing and the climate impact of this vegetation change would eventually switch to a net cooling after about 120 years. Note that the simulated C fluxes over winter are not well-constrained by field data at this time.

4. Discussion

4.1 Validation of DNDC

In this study, we applied the new version of DNDC to simulate soil freeze/thaw dynamics and C fluxes across three typical land cover types (i.e., Palsa, Sphagnum, and Eriophorum) at Stordalen, Sweden, which are considered to represent a gradient of permafrost thaw (Johansson T. et al., 2006; Bäckstrand et al., 2010). Both field observations and DNDC simulations showed significant differences in C fluxes across these three land cover types and the simulated rates of seasonal cumulative C fluxes were comparable with the corresponding measurements for most cases (Tables 3 and 4). These results indicate that the model successfully captured the differences in

C fluxes among these land cover types. In addition, the model generally captured the magnitudes and temporal dynamics of soil thaw, NEE, and CH_4 fluxes (Figures 2, 3, and 4). The model validation suggests that the enhanced DNDC potentially can be used to predict impacts of permafrost thaw, but cannot yet independently simulate subsequent changes in soil hydrology and vegetation, which influence C dynamics in northern peatlands. We also note some discrepancies between the modeled results and the field measurements.

Compared to daily observations of NEE, DNDC overestimated CO_2 uptake rates (i.e., predicted more negative NEE) on a few days during the growing seasons (Figure 3), which may have resulted from over-prediction of photosynthesis, causing DNDC to predict higher NPP. Because meteorological data at the ANS (10 km northwest of Stordalen) were used to support the simulations and photosynthesis is closely related to climate factors, deviations in predicting daily variability in photosynthesis may be caused by lacking site-specific data. Local observations also demonstrated that meteorological conditions were different between Stordalen and ANS (Olefeldt and Roulet, 2012; Rydén, 1980). These differences inevitably affected model simulations of C fluxes. We further calculated the $RMSE_S$ and $RMSE_U$ for daily NEE (Table 5). The results demonstrate that systematic errors accounted for 11%, 25%, and 23% of the mean-square errors in daily NEE at the Palsa, Sphagnum, and Eriophorum sites, respectively. Therefore the discrepancies between the modeled and measured NEE could be primarily attributed to random components, including absence of site-specific data. However, we also note systematic discrepancies between the modeled and observed NEE at both the Sphagnum and Eriophorum sites. Inconsistent with field data in other years, high net uptake rates of CO_2 occurred at the Sphagnum

site during 25 May to 22 June in 2003 (Figure 3h-n), even though solar radiation, air temperature, and soil temperature were low (Figure 1) and soil thaw depth was shallow (Figure 2h), causing DNDC to predict lower uptake rates. At the Eriophorum site, the model predicted an increasing trend of net CO_2 uptake (Figure 3p) from late May to the end of June in 2004 because of the increases in solar radiation, air temperature, and soil thaw depth, while the field observations showed persistent low net CO_2 uptake rates. Further studies are needed to clarify the differences in seasonal characteristics of NEE between 2003 and other years at the Sphagnum site, as well as the inconsistencies between the predictions and observations.

DNDC approximately matched the observed daily CH_4 fluxes at both the Sphagnum and Eriophorum sites (Figure 4). However, we also note a few inconsistencies between the simulations and observations (e.g., in 2003 at the Sphagnum site and in 2008 at the Eriophorum site). Model parameters for soil and vegetation characteristics were derived from a number of studies done at Stordalen since the International Biosphere Program in the early 1970s (Sonesson et al., 1980). Because these parameters have strong influences on soil climate, plant growth, and soil biogeochemistry in DNDC, potential biases in inputs could affect model results, including CH_4 fluxes. The calculations of $RMSE_S$ and $RMSE_U$ (Table 5) also demonstrate that most of the mean-square errors in daily CH_4 fluxes were attributable to random errors, including deviations resulted from biases in model inputs, at both the Sphagnum (76%) and Eriophorum (89%) sites.

In addition, it should be noted that the modeled C fluxes over winter periods remain uncertain because observations utilized for model validation were primarily available

635 during growing seasons. DNDC simulations demonstrated that C fluxes during
636 non-growing season substantially contributed to annual C fluxes at Stordalen. During
637 2003 to 2009, the means of accumulated CO_2 emissions over non-growing seasons
638 were 342, 32.8, and 101 kg CO_2-C ha^{-1}, respectively, at the Palsa, Sphagnum, and
639 Eriophorum sites. Local field studies also indicated that net CO_2 emissions over
640 winter periods significantly contributed to annual NEE at both dry and wet areas
641 (Bäckstrand et al., 2010; Christensen et al., 2012) and accumulation of net CO_2
642 emissions during winter may have made the dry Palsa site a net annual CO_2 source
643 (Bäckstrand et al., 2010). The simulations of average accumulated CH_4 fluxes over
644 non-growing seasons were 9.8 and 13.8 kg CH_4-C ha^{-1} at the Sphagnum and
645 Eriophorum sites; representing 30% and 13% of mean annual emissions. At the wet
646 area dominated by tall graminoid vegetation, field measurements demonstrated that
647 CH_4 emissions over winter accounted for approximately 19% of the annually emitted
648 CH_4 (Jackowicz-Korczyński et al., 2010). These results indicate that further tests are
649 necessary to verify the model's predictions of C fluxes during winter periods.
650
651 Although the modeled C fluxes were tested against field measurements with
652 encouraging results, we note that uncertainty may exist in simulating individual
653 processes in C transformations. For example, methane flux is predicted by DNDC as
654 the net result of CH_4 production, oxidation, and transport processes. Validating
655 simulations of CH_4 emission against field measurements did not evaluate the
656 DNDC's simulation of these three processes individually. One approach for
657 testing/constraining simulation of the individual processes is to include stable
658 isotopes and isotope fractionation during the processes of methanogenesis (acetate
659 fermentation and CO_2 reduction), methane oxidation, and methane transport (e.g.,

660 Chanton et al., 2005; Corbett et al., 2013). This is planned for future model
661 development.
662
663 **4.2 Permafrost thaw and C fluxes**
664 Our modeled results provide some indications on how C fluxes will change with
665 ongoing permafrost thaw at Stordalen. If the Palsa evolves into Sphagnum or
666 Eriophorum during permafrost thaw, the mire may be able to sequester more
667 atmospheric C, considering the higher rates of net C uptake shown at the Sphagnum
668 or Eriophorum sites (Figure 6b). However, increases of net C uptake were positively
669 correlated with increases of CH_4 emissions across the thaw gradient at Stordalen
670 (Figure 6), indicating that permafrost thaw will generate a tradeoff of GHG. If the net
671 impact is calculated using the GWP methodology (e.g., Shine et al., 1990), the
672 balance depends on the relative rate of changes in CO_2 uptake and CH_4 emissions and
673 the time horizon chosen for the GWP calculation (e.g., Frolking and Roulet, 2007;
674 Whiting and Chanton, 2001).
675
676 By applying the modeled C fluxes to the areal changes of land cover types at
677 Stordalen, we estimated that the net impact due to the vegetation change is a net CO_2
678 equivalent emission of 527 kg CO_2-eq. yr^{-1} from 1970 to 2000 at Stordalen. However,
679 it should be noted that this result was calculated by assuming constant annual
680 emissions (equal to the means simulated by DNDC from 2003 to 2009) between 1970
681 and 2000 and the modeled results showed obvious inter-annual variability in both
682 NEE and CH_4 fluxes (Figure 6), and it is not known when during 1970-2000 the
683 land-cover change occurred. If the net impact is calculated by considering the
684 inter-annual variability of C fluxes, the estimation of a net CO_2 equivalent emission

from 1970 to 2000 is not significant (P = 0.07) higher than zero. Johansson T. et al. (2006) also used a 100-year GWP value for methane, but treated their 'wet' cover somewhat differently – equivalent to 'semi-wet' (Sphagnum) for NEE due to similarity in vegetation composition, but with a higher value for CH_4 emission as it was an inundated area. Because the 'wet' area was nearly 30% of the study region and expanded from 1970 to 2000, Johansson T. et al. (2006) estimated that the mire was a GHG source in terms of CO_2 equivalents to the atmosphere, and they reported an increase of 47% in net radiative forcing from 1970 to 2000 by considering the fluxes during growing season. Our analysis estimated that the mire was a GHG sink due to a lower value for CH_4 emission in 'wet' areas, and yielded an overall decrease of 27% in net radiative cooling from 1970 to 2000. The differences and uncertainties in these interpretations illustrate an important scaling challenge – how many land cover classes are needed and what are the most important distinctions to consider? This can be evaluated in future analyses by comparison of up-scaling flux by aerial fractions of land cover with multi-year eddy covariance tower fluxes. Flux towers are now operating at Stordalen under the European Integrated Carbon Observation System (ICOS) program (Paris et al., 2012).

4.3 Modeling impacts of permafrost thaw on C fluxes

Modeling impacts of permafrost thaw on C fluxes is in a very early stage, and much additional work is required for a more complete treatment of all of the processes involved. As shown in this and other studies (e.g., Olefeldt et al., 2013), NEE and CH_4 fluxes are strongly controlled by soil water regime and vegetation characteristics, which stresses the importance of considering changes in soil hydrology and vegetation when predicting responses of C turnover to climate change in permafrost

ecosystems. Although changes in wetland cover and vegetation have been observed along with permafrost degradation in northern peatlands (e.g., Goetz et al., 2011; Smith et al., 2005), most modeling work that predicts impacts of climate change on C turnover are based on static distribution of wetlands and vegetation (Bohn and Lettenmaier, 2010). Therefore biases may result from neglecting changes in water table regime and vegetation transitions along with permafrost thaw. In this study, we determined different soil water conditions for the three land cover types at Stordalen by combining the observed WTD and the hydrological module of DNDC. The required hydrological parameters were estimated by calibrating against WTD datasets (Table 1). While these parameters were empirically determined, they are consistent with the general topography of Stordalen, with the Palsa surface elevated 0.5-2.0 m above the Eriophorum surface, and the Sphagnum surface at intermediate elevation (Olefeldt and Roulet, 2012). However, it should be noted that sufficient WTD data are required for calibrating these hydrological parameters if the model is to be applied to other peatlands. Although different WTD and vegetation characteristics were used as inputs for different land cover types to represent changes in soil water regime and vegetation along with permafrost thaw at Stordalen, it would be ideal to incorporate these changes dynamically into the model's framework for better understanding how permafrost thaw affect landscape wetness and how this in turn affect vegetation and C fluxes. Our efforts of incorporating a permafrost model should have set a sound basis for the model to incorporate the processes related to changes in soil water regime and vegetation along with permafrost thaw, although important additional processes needed in a comprehensive biogeochemical model fully functional for northern ecosystems.

5. Conclusions

Climate warming and associated permafrost degradation are expected to have significant impacts on the C balance of permafrost ecosystems but the magnitude is uncertain. We incorporated a permafrost model, NEST, into a biogeochemical model, DNDC, to model C dynamics in high-latitude ecosystems. The enhanced DNDC model was applied to assess effects of permafrost thaw on C fluxes of a sub-arctic peatland at Stordalen, Sweden. DNDC simulated soil freeze/thaw dynamics and C fluxes across three typical land cover types (i.e., Palsa, Sphagnum, and Eriophorum) at Stordalen, which span a gradient in the processes of permafrost thaw. Model results were tested against multi-year field measurements. The model validation indicates that DNDC was able to capture differences in seasonal soil thaw, NEE, and CH_4 fluxes across the Palsa, Sphagnum, and Eriophorum sites at Stordalen. In addition, the simulated magnitudes and temporal dynamics of soil thaw, NEE, and CH_4 fluxes were in general agreement with field measurements. Consistent with the results from field studies, the modeled C fluxes across the permafrost thaw gradient demonstrate that permafrost thaw and the associated changes in soil hydrology and vegetation increase net uptake of C from atmosphere, but also increase the radiative forcing impacts on climate due to increased CH_4 emission. By using the modeled annual C fluxes and reported areas of vegetation cover in 1970 and 2000, we estimated that the Stordalen mire was a net GHG sink (using a 100-year GWP value for methane) and yielded an overall decrease of 27% in net radiative cooling from 1970 to 2000.

Acknowledgements

This study was supported by the NASA Terrestrial Ecology Program (NNX09AQ36G), the US Department of Energy (DE-SC0004632), and the US National Science Foundation (ARC-1021300). We thank the Abisko Scientific Research Station for providing the meteorological data. We thank N. T. Roulet and an anonymous reviewer for comments and suggestions that improved the manuscript.

References

ACIA: Arctic climate impact assessment: scientific report, Cambridge University Press, New York, 2005.

Aerts, R., Wallén, B., and Malmer, N.: Growth-limiting nutrients in *Sphagnum*-dominated bogs subject to low and high atmospheric nitrogen supply, J. Ecol., 80, 131-140, 1992.

Aerts, R., Wallén, B., Malmer, N., and de Caluwe, H.: Nutritional constraints on *Sphagnum*-growth andpotential decay in northern peatlands, J. Ecol., 89, 292-299, 2001.

Avis, C. A., Weaver, A. J., and Meissner, K. J.: Reduction in areal extent of high-latitude wetlands in response to permafrost thaw, Nat. Geosci., 4, 444-448, 2011.

Åkerman, H. J. and Johansson, M.: Thawing permafrost and thicker active layers in sub-arctic Sweden, Permafrost Periglac., 19, 279-292, 2008.

Bäckstrand, K., Crill, P. M., Mastepanov, M., Christensen, T. R., and Bastviken, D.: Total hydrocarbon flux dynamics at a subarctic mire in northern Sweden, J. Geophys. Res., 113, G03026, doi:10.1029/2008JG000703, 2008.

Bäckstrand, K., Crill, P. M., Jackowicz-Korczyński, M., Mastepanov, M., Christensen, T. R., and Bastviken, D.: Annual carbon gas budget for a subarctic peatland, Northern Sweden, Biogeosciences, 7, 95-108, 2010.

Bohn, T. J. and Lettenmaier, D. P.: Systematic biases in large-scale estimates of wetland methane emissions arising from water table formulations, Geophys. Res. Lett., 37, L22401, doi: 10.1029/2010GL045450, 2010.

Callaghan, T. V., Bergholm, F., Christensen, T. R., Jonasson, C., Kokfelt, U., and Johansson, M.: A new climate era in the sub-Arctic: Accelerating climate changes

789 and multiple impacts, Geophys. Res. Lett., 37, L14705, doi:
790 10.1029/2009GL042064, 2010.
791 Chanton, J. P., Chasar, L., Glaser, P. H., and Siegel, D. I.: Carbon and hydrogen
792 isotopic effects in microbial methane from terrestrial environments, In: Stable
793 isotopes and biosphere-atmosphere interactions: processes and biological controls,
794 Flanagan, L. B., Ehleringer, J. R., and Pataki, D. E., Elsevier, Amsterdam, 85-105,
795 2005.
796 Christensen, T. R., Johansson, T., Åkerman, H. J., Mastepanov, M., Malmer, N.,
797 Friborg, T., Crill, P., and Svensson, B. H.: Thawing sub-arctic permafrost: effects
798 on vegetation and methane emissions, Geophys. Res. Lett., 31, L04501, doi:
799 10.1029/2003GL018680, 2004.
800 Christensen, T. R., Jackowicz-Korczyński, M., Aurela, M., Crill, P., Heliasz, M.,
801 Mastepanov, M., and Friborg, T.: Monitoring the multi-year carbon balance of a
802 subarctic palsa mire with micrometeorological techniques, Ambio, 41, 207-217,
803 2012.
804 Clauser, C. and Huenges, E.: Thermal conductivity of rocks and minerals, In: Rock
805 Physics & Phase Relations: A Handbook of Physical Constants, Ahrens, T. J.,
806 AGU, Washington, D. C., 105-126, 1995.
807 Corbett, J. E., Tfaily, M. M., Burdige, D. J., Cooper, W. T., Glaser, P. H., and Chanton,
808 J. P.: Partitioning pathways of CO_2 production in peatlands with stable carbon
809 isotopes, Biogeochemistry, 114, 327-340, doi: 10.1007/s10533-012-9813-1, 2013.
810 Davis, N.: Permafrost: A Guide to Frozen Ground in Transition, University of Alaska
811 Press, Fairbanks, AK, 2001.
812 Dorrepaal, E., Toet, S., van Logtestijn, R. S. P., Swart, E., van de Weg, M. J.,
813 Callaghan, T. V., and Aerts, R.: Carbon respiration from subsurface peat

accelerated by climate warming in the subarctic, Nature, 460, 616-619, 2009.

Frolking, S., Roulet, N., and Fuglestvedt, J.: How northern peatlands influence the Earth's radiative budget: Sustained methane emission versus sustained carbon sequestration, J. Geophys. Res., 111, G01008, doi:10.1029/2005JG000091, 2006.

Frolking, S. and Roulet, N. T.: Holocene radiative forcing impact of northern peatland carbon accumulation and methane emissions, Glob. Change Biol., 13, 1079-1088, 2007.

Frolking, S., Talbot, J., Jones, M., Treat, C. C., Kauffman, J. B., Tuittila, E. S., and Roulet, N. T.: Peatlands in the Earth's 21st century climate system, Environ. Rev., 19, 371-396, 2011.

Fumoto, F., Kobayashi, K., Li, C., Yagi, K., and Hasegawa, T.: Revising a process-based biogeochemistry model (DNDC) to simulate methane emission from rice paddy fields under various residue management and fertilizer regimes, Glob. Change Biol., 14, 382-402, 2008.

Goetz, S. J., Epstein, H. E., Bhatt, U. S., Jia, G. J., Kaplan, J. O., Lischke, H., Yu, Q., Bunn, A., Lloyd, A. H., Alcaraz-Segura, D., Beck, P. S. A., Comiso, J. C., Raynolds, M. K., and Walker, D. A.: Recent changes in arctic vegetation: satellite observations and simulation model predictions, In: Eurasian arctic land cover and land use in a changing climate, Gutman, G. and Reissell, A., Springer, Nertherlands, 9-36, 2011.

IPCC: Climate change 2007: the physical science basis, In: Contribution of working group I to the fourth assessment report of the Intergovernmental Panel on Climate Change: "The Physical Science Basis", Solomon, S., Qin, D., Manning, M., Chen, Z., Marquis, M., Averyt, K. B., Tignor, M., and Miller, H. L., Cambridge University Press, Cambridge, 2007.

839 Jackowicz-Korczyński, M., Christensen, T. R., Bäckstrand, K., Crill, P. M., Friborg, T.,
840 Mastepanov, M., and Ström, L.: Annual cycle of methane emission from a
841 subarctic peatland, J. Geophys. Res., 115, G02009, doi:10.1029/2008JG000913,
842 2010.
843 James, M., Lewkowicz, A. G., Smith, S. L., and Miceli, C. M.: Multi-decadal
844 degradation and persistence of permafrost in the Alaska Highway corridor,
845 northwest Canada, Environ. Res. Lett., 8, 045013,
846 doi:10.1088/1748-9326/8/4/045013, 2013.
847 Johansson, M., Christensen, T. R., Åkerman, J. H., and Callaghan, T. V.: What
848 determines the current presence or absence of permafrost in the torneträsk region,
849 a sub-arctic landscape in northern Sweden, Ambio, 35, 190-197, 2006.
850 Johansson, T., Malmer, N., Crill, P. M., Friborg, T., Åkerman, J., Mastepanov, M., and
851 Christensen, T. R.: Decadal vegetation changes in a northern peatland, greenhouse
852 gas fluxes and net radiative forcing, Glob. Change Biol., 12, 2,352-2,369, doi:
853 10.1111/j.1365-2486.2006.01267.x, 2006.
854 Kirschke, S., Bousquet, P., Ciais, P., Saunois, M., Canadell, J. G., Dlugokencky, E. J.,
855 Bergamaschi, P., Bergmann, D., Blake, D. R., Bruhwiler, L., Cameron-Smith, P.,
856 Castaldi, S., Chevallier, F., Feng, L., Fraser, A., Heimann, M., Hodson, E. L.,
857 Houweling, S., Josse, B., Fraser, P. J., Krummel, P. B., Lamarque, J., Langenfelds,
858 R. L., Le Quere, C., Naik, V., O'Doherty, S., Palmer, P. I., Pison, I., Plummer, D.,
859 Poulter, B., Prinn, R. G., Rigby, M., Ringeval, B., Santini, M., Schmidt, M.,
860 Shindell, D. T., Simpson, I. J., Spahni, R., Steele, L. P., Strode, S. A., Sudo, K.,
861 Szopa, S., van der Werf, G. R., Voulgarakis, A., van Weele, M., Weiss, R. F.,
862 Williams, J. E., and Zeng, G.: Three decades of global methane sources and sinks,
863 Nat. Geosci., 6, 813-823, doi: 10.1038/NGEO1955, 2013.

Koven, C. D., Ringeval, B., Friedlingstein, P., Ciais, P., Cadule, P., Khvorostyanov, D., Krinner, G., and Tarnocai, C.: Permafrost carbon-climate feedbacks accelerate global warming, P. Natl. Acad. Sci. USA, 108, 14,769-14,774, 2011.

Li, C.: Modeling trace gas emissions from agricultural ecosystems, Nutr. Cycl. Agroecos., 58, 259-276, doi:10.1023/A:1009859006242, 2000.

Li, C.: Quantifying greenhouse gas emissions from soils: scientific basis and modeling approach, Soil Sci. Plant Nutr., 53, 344-352, 2007.

Li, C., Frolking, S., and Frolking, T. A.: A model of nitrous oxide evolution from soil driven by rainfall events: 1. Model structure and sensitivity, J. Geophys. Res., 97, 9,759-9,776, 1992a.

Li, C., Frolking, S., and Frolking, T. A.: A model of nitrous oxide evolution from soil driven by rainfall events: 2. Model applications, J. Geophys. Res., 97, 9,777-9,783, 1992b.

Li, C., Aber, J., Stange, F., Butterbach-Bahl, K., and Papen, H.: A process-oriented model of N_2O and NO emissions from forest soils: 1. Model development, J. Geophys. Res., 105, 4,365-4,384, 2000.

Li, C., Salas, W., Zhang, R., Krauter, C., Rotz, A., and Mitloehner, F.: Manure-DNDC: a biogeochemical process model for quantifying greenhouse gas and ammonia emissions from livestock manure systems, Nutr. Cycl. Agroecos., 93, 163-200, doi: 10.1007/s10705-012-9507-z, 2012.

Lund, M., Lafleur, P. M., Roulet, N. T., Lindroth, A., Christensen, T. R., Aurela, M., Chojnicki, B. H., Flanagan, L. B., Humphreys, E. R., Laurila, T., Oechel, W. C., Olejnik, J., Rinne, J., Schubert, P., and Nilsson, M. B.: Variability in exchange of CO_2 across 12 northern peatland and tundra sites, Glob. Change Biol., 16, 2,436-2,448, 2010.

889 Majorowicz, J. and Wybraniec, S.: New terrestrial heat flow map of Europe after
890 regional paleoclimatic correction application, Int. J. Earth Sci., 100, 881-887,
891 2011.
892 Malmer, N. and Wallén, B.: Peat formation and mass balance in subarctic
893 ombrotrophic peatlands around Abisko, northern Scandinavia, Ecol. Bull., 45,
894 79-92, 1996.
895 Malmer, N., Johansson, T., Olsrud, M., and Christensen, T. R.: Vegetation, climatic
896 changes and net carbon sequestration in a North-Scandinavian subarctic mire over
897 30 years, Glob. Change Biol., 11, 1895-1909, 2005.
898 McGuire, A. D., Anderson, L. G., Christensen, T. R., Dallimore, S., Guo, L., Hayes, D.
899 J., Helmann, M., Lorenson, T. D., Macdonald, R. W., and Roulet, N.: Sensitivity
900 of the carbon cycle in the Arctic to climate change, Ecol. Monogr., 79, 523-555,
901 2009.
902 Moriasi, D. N., Arnold, J. G., Van Liew, M. W., Bingner, R. L., Harmel, R. D., and
903 Veith, T. L.: Model evaluation guidelines for systematic quantification of accuracy
904 in watershed simulations, T. ASABE, 50, 885-900, 2007.
905 Nungesser, M. K.: Modelling microtopography in boreal peatlands: hummocks and
906 hollows, Ecol. Model., 165, 175-207, 2003.
907 Olefeldt, D. and Roulet, N. T.: Effects of permafrost and hydrology on the composition
908 and transport of dissolved organic carbon in a subarctic peatland complex, J.
909 Geophys. Res., 117, G01005, doi:10.1029/2011JG001819, 2012.
910 Olefeldt, D., Roulet, N. T., Bergeron, O., Crill, P. M., Bäckstrand, K., and Christensen,
911 T. R.: Net carbon accumulation of a high-latitude permafrost palsa mire similar to
912 permafrost-free peatlands, Geophys. Res. Lett., 39, L03501,
913 doi:10.1029/2011GL050355, 2012.

914 Olefeldt, D., Turetsky, M. R., Crill, P. M., and McGuire, A. D.: Environmental and
915 physical controls on northern terrestrial methane emissions across permafrost
916 zones, Glob. Change Biol., 19, 589-603, 2013.
917 Olsrud, M. and Christensen, T. R.: Carbon partitioning in a wet and a semiwet
918 subarctic mire ecosystem based on in situ ^{14}C pulse-labelling, Soil Biol. Biochem.,
919 43, 231-239, 2011.
920 Öquist, M. G. and Svensson, B. H.: Vascular plants as regulators of methane emissions
921 from a subarctic mire ecosystem, J. Geophys. Res., 107, 4580,
922 doi:10.1029/2001JD001030, 2002.
923 Payette, S., Delwaide, A., Caccianiga, M., and Beauchemin, M.: Accelerated thawing
924 of subarctic peatland permafrost over the last 50 years, Geophys. Res. Lett., 31,
925 L18208, doi: 10.1029/2004GL020358, 2004.
926 Paris, J. D., Ciais, P., Rivier, L., Chevallier, F., Dolman, H., Flaud, J. M., Garrec, C.,
927 Gerbig, C., Grace, J., Huertas, E., Johannessen, T., Jordan, A., Levin, I., Papale, D.,
928 Valentini, R., Watson, A., Vesala, T., and ICOS-PP consortium: Integrated Carbon
929 Observation System, Geophysical Research Abstracts, 14, EGU2012-12397, 2012.
930 Quinton, W., Hayashi, M., and Chasmer, L.: Permafrost-thaw-induced land-cover
931 change in the Canadian subarctic: implications for water resources, Hydrol.
932 Process., 25, 152-158, 2011.
933 Riseborough, D., Shiklomanov, N., Etzelmüller, B., Gruber, S., and Marchenko, S.:
934 Recent Advances in Permafrost Modelling, Permafrost Periglac., 19, 137-156,
935 2008.
936 Rosswall, T., Flower-Ellis, J. G. K., Johansson, L. G., Jonsson, S., Rydén, B. E., and
937 Sonesson, M.: Stordalen (Abisko), Sweden, Ecol. Bull., 20, 265-294, 1975.
938 Rydén, B. E.: Climatic representativeness of a project period: epilogue of a tundra

939 study, Ecol. Bull., 30, 55-62, 1980.
940 Rydén, B. E. and Kostov, L.: Thawing and freezing in tundra soils, Ecol. Bull., 30,
941 251-281, 1980.
942 Rydén, B. E., Fors, L., and Kostov, L.: Physical properties of the tundra soil-water
943 system at Stordalen, Abisko, Ecol. Bull., 30, 27-54, 1980.
944 Sachs, T., Giebels, M., Boike, J., and Kutzbach, L.: Environmental controls of CH_4
945 emission from polygonal tundra on the micro-site scale, Lena River Delta, Siberia,
946 Glob. Change Biol., 16, 3,096-3,110, 2010.
947 Schneider von Diemling, T., Meinshausen, M., Levermann, A., Huber, V., Frieler, K.,
948 Lawrence, D. M., and Brovkin, V.: Estimating the near-surface permafrost-carbon
949 feedback on global warming, Biogeosciences, 9, 649-665, 2012.
950 Schuur, E. A. G., Bockheim, J., Canadell, J. G., Euskirchen, E., Field, C. B.,
951 Goryachkin, S. V., Hagemann, S., Kuhry, P., Lafleur, P. M., Lee, H., Mazhitova, G.,
952 Nelson, F. E., Rinke, A., Romanovsky, V. E., Shiklomanov, N., Tarnocai, C.,
953 Venevsky, S., Vogel, J. G., and Zimov, S. A.: Vulnerability of permafrost carbon to
954 climate change: implications for the global carbon cycle, BioScience, 58, 701-714,
955 2008.
956 Schuur, E. A. G., Vogel, J. G., Grummer, K. G., Lee, H., Sickman, J. O., and
957 Osterkamp, T. E.: The effect of permafrost thaw on old carbon release and net
958 carbon exchange from tundra, Nature, 459, 556-559, 2009.
959 Schuur, E. A. G., Benjamin, A., and Permafrost Carbon Network: High risk of
960 permafrost thaw, Nature, 480, 32-33, 2011.
961 Shine, K. P., Derwent, R. G., Wuebbles, D. F., and Morcrette, J. J.: Radiative forcing of
962 climate, In: Climate Change: The IPCC Scientific Assessment, Houghton, J. T.,
963 Jenkins, G. J., and Ephraums, J. J., Cambridge University Press, Cambridge, UK,

964 41-68, 1990.
965 Smith, L. C., Sheng, Y., McDonald, G. M., and Hinzman, L. D.: Disappearing arctic
966 lakes, Science, 308, 1429, doi: 10.1126/science.1108142,2005.
967 Sonneson, M., Jonsson, S., Rosswall, T., and Ryden, B. E.: The Swedish IBP/PT tundra
968 biome project: objectives – planning – site, Ecol. Bull., 30, 7-25, 1980.
969 Stange, F., Butterbach-Bahl, K., Papen, H., Zechmeister-Boltenster, S., Li, C., and
970 Aber, J.: A process-oriented model of N_2O and NO emissions from forest soils: 2.
971 Sensitivity analysis and validation, J. Geophys. Res., 105, 4,385-4,398, 2000.
972 Ström, L. and Christensen, T. R.: Below ground carbon turnover and greenhouse gas
973 exchanges in a sub-arctic wetland, Soil Biol. Biochem., 39, 1,689-1,698, 2007.
974 Tarnocai, C., Canadell, J. G., Schuur, E. A. G., Kuhry, P., Mazhitova, G., and Zimov, S.:
975 Soil organic carbon pools in the northern circumpolar permafrost region, Global
976 Biogeochem. Cy., 23, GB2023, doi:10.1029/2008GB003327, 2009.
977 Waelbroeck, C.: Climate-soil processes in the presence of permafrost: a systems
978 modelling approach, Ecol. Model., 69, 185-225, 1993.
979 Wania, R., Ross, I., and Prentice, I. C.: Integrating peatlands and permafrost into a
980 dynamicglobal vegetation model: 1. Evaluation and sensitivity of physical land
981 surface processes, Global Biogeochem. Cy., 23, GB3014,
982 doi:10.1029/2008GB003412, 2009a.
983 Wania, R., Ross, I., and Prentice, I. C.: Integrating peatlands and permafrost into a
984 dynamic global vegetation model: 2. Evaluation and sensitivity of vegetation and
985 carbon cycle processes, Global Biogeochem. Cy., 23, GB3015,
986 doi:10.1029/2008GB003413, 2009b.
987 Whiting, G. J. and Chanton, J. P.: Greenhouse carbon balance of wetlands: methane
988 emission versus carbon sequestration, Tellus B, 53, 521-528, 2001.

Williams, P. J. and Smith, M. W.: The Frozen Earth: Fundamentals of Geocryology, Cambridge University Press, Cambridge, UK, 1989.

Willmott, C. J.: Some comments on the evaluation of model performance, B. AM. Meteorol. Soc., 63, 1,309-1,313, 1982.

Willmott, C. J., Ackleson, S. G., Davis, R. E., Feddema, J. J., Klink, K. M., Legates, D. R., O'Donnell, J., and Rowe, C. M.: Statistics for the evaluation and comparison of models, J. Geophys. Res., 90, 8,995-9,005, 1985.

Yu, Z., Loisel, J., Brosseau, D. P., Beilman, D. W., and Hunt, S. J.: Global peatland dynamics since the Last Glacial Maximum, Geophys. Res. Lett., 37, L13402, doi:10.1029/2010GL043584, 2010.

Zhang, Y., Li, C., Trettin, C. C., Li, H., and Sun, G.: An integrated model of soil, hydrology and vegetation for carbon dynamics in wetland ecosystems, Global Biogeochem. Cy., 16, 1061, doi: 10.1029/2001GB001838, 2002.

Zhang, Y., Chen, W., and Cihlar, J.: A process-based model for quantifying the impact of climate change on permafrost thermal regimes, J. Geophys. Res., 108, 4695, doi:10.1029/2002JD003354, 2003.

Zhang, Y., Chen, W., Smith, S. L., Riseborough, D. W., and Cihlar, J.: Soil temperature in Canada during the twentieth century: complex responses to atmospheric climate change, J. Geophys. Res., 110, D03112, doi:10.1029/2004JD004910, 2005.

Zhang, Y., Sachs, T., Li, C., and Boike, J.: Upscaling methane fluxes from closed chambers to eddy covariance based on a permafrost biogeochemistry integrated model, Glob. Change Biol., 18, 1,428-1,440, doi: 10.1111/j.1365-2486.2011.02587.x, 2012.

Zhang, Y., Wang, X., Fraser, R., Olthof, I., Chen, W., Mclennan, D., Ponomarenko, S., and Wu, W.: Modelling and mapping climate change impacts on permafrost at

high spatial resolution for an Arctic region with complex terrain, The Cryosphere, **7**, 1121-1137, doi:10.5194/tc-7-1121-2013, 2013.

Zhuang, Q., Romanovsk, V. E., and McGuire, A. D.: Incorporation of a permafrost model into a large-scale ecosystem model: Evaluation of temporal and spatial scaling issues in simulating soil thermal dynamics, J. Geophys. Res., 106, 33, 649-33, 670, 2001.

Zhuang, Q., Melillo, J. M., Kicklighter, D. W., Prinn, R. G., McGuire, A. D., Steudler, P. A., Felzer, B. S., and Hu, S.: Methane fluxes between terrestrial ecosystems and the atmosphere at northern high latitudes during the past century: a retrospective analysis with a process-based biogeochemistry model, Global Biogeochem. Cy., 18, GB3010, doi:10.1029/2004GB002239, 2004.

Zhuang, Q., Melillo, J. M., Sarofim, M. C., Kicklighter, D. W., McGuire, A. D., Felzer, B. S., Sokolov, A., Prinn, R. G., Steudler, P. A., and Hu, S.: CO_2 and CH_4 exchanges between land ecosystems and the atmosphere in northern high latitudes over the 21st century, Geophys. Res. Lett., 33, L17403, doi: 10.1029/2006GL026972, 2006.

Tables

Table 1 The hydrological parameters used for modeling lateral flows[a].

Sites	SIR	SOD (m)	SOR	GOD (m)	GOR
Sphagnum	1.0	0	1.0	0.25	0.01
Eriophorum	2.0	-0.05	0.3	0.05	0.01

[a] SIR, surface inflow rate, the fraction (m m^{-1}) of rainfall (or water from snow melt) flowing into the site from its surroundings; SOD, surface outflow depth, the water table (WT) depth (positive for below-ground and negative for above-ground) above which surface lateral outflow occurs; SOR, surface outflow rate, the fraction (m m^{-1}) of water above the SOD which will be lost as surface outflow per day; GOD, ground outflow depth, the deepest WT depth above which ground outflow occurs; GOR, ground outflow rate, the fraction (m m^{-1}) of water above the GOD which will be lost as ground outflow per day. These hydrological parameters were determined by calibrating against datasets of water table depth.

1043 **Table 2** The physiological parameters used for simulating plant growth.

Sites	MP[a]	SRF[b]	C/N[c]	TDD[d]	WR[e]	Vascularity	NFI[f]
Palsa	1000	0.35/0.65	90	1500	100	0	1.0
Sphagnum	1200	0.7/0.3	90	1500	100	0	1.1
Eriophorum	2500	0.5/0.5	90	1500	100	1	1.5

1044 [a] MP, the maximum productivity under optimum growing conditions (kg C ha^{-1}). The
1045 values were estimated from Rosswall et al. (1975), Malmer and Walleń (1996), and
1046 Malmer et al. (2005).

1047 [b] SRF, the shoot and root fractions. The values were estimated from Ström and
1048 Christensen (2007), Olsurd and Christensen (2011). Note that the vegetation at the
1049 Sphagnum site is not 100% moss.

1050 [c] C/N, carbon to nitrogen ratio of the plant biomass. The values were estimated from
1051 Aerts et al. (1992, 2001).

1052 [d] TDD, the required accumulated air temperature heat sum above a 0 °C threshold
1053 during the growing season (unit: °C • day) for full vegetation growth.

1054 [e] WR, amount of water required by the plant (g water g^{-1} dry matter).

1055 [f] NFI, index of biological nitrogen fixation.

1056

Table 3 Comparison of the modeled (M) and observed (O) net ecosystem exchanges (NEE, in kg C ha^{-1}) of CO_2 during growing periods at the Palsa, Sphagnum, and Eriophorum sites[a].

Year	Palsa			Sphagnum			Eriophorum		
	O[b]	M	RRMSE[c]	O	M	RRMSE	O	M	RRMSE
2003	-330[264]	-414	25	-394[59]	-326	17	-1118[219]	-1078	4
2004	-241[269]	-265	10	-441[73]	-452	2	-815[449]	-870	7
2005	-338[369]	-347	3	-525[69]	-521	1	-741[450]	-980	32
2006	-386[283]	-319	17	-356[27]	-330	8	-1034[94]	-1019	1
2007	-338[187]	-353	4	-436[114]	-424	3	-930[208]	-980	5
2008	-399[263]	-328	18	-264[79]	-288	9	-471[76]	-571	21
2009	-435[129]	-380	13	-212[75]	-203	4	-270[59]	-365	35

[a] The growing period in this study is defined as the periods during which measurements of continuous net CO_2 uptake were available. To calculate the total NEE over the growing period in each year, fluxes for the days lacking measurements were determined using the arithmetic mean fluxes of the two closest days when observations were performed. Daily fluxes from either direct measurements or gap-filling were then summed up to calculate the growing period cumulative NEE.

[b] Each figure number within the bracket is the standard deviation of three (Palsa and Sphagnum) or two (Eriophorum) replicate auto-chamber plots.

[c] RRMSE, relative root mean squared error, %.

Table 4 Comparison of the modeled (M) and observed (O) CH_4 fluxes (in kg C ha^{-1}) during six study periods at the Sphagnum and Eriophorum sites[a].

Year	Sphagnum			Eriophorum		
	O[b]	M	RRMSE[c]	O	M	RRMSE
2003	17.2[5.2]	12.2	29	91.8[10.5]	76.4	17
2004	30.6[8.0]	24.3	21	121[14.7]	105	13
2005	25.1[4.7]	24.1	4	108[60.6]	101	7
2007	30.4[7.5]	35.7	18	116[22.2]	113	3
2008	9.7[4.2]	13.1	35	57.9[4.42]	45.3	22
2009	23.2[7.5]	27.5	18	111[21.7]	101	9

[a] The study period is the span during which continuous measurements of daily CH_4 fluxes were available. To calculate the total CH_4 emissions over the sampling period in each year, fluxes for the days lacking measurements were determined using the arithmetic mean fluxes of the two closest days when observations were performed. Daily fluxes from either direct measurements or gap-filling were then summed up to calculate the growing period cumulative CH_4 emissions.

[b] Each figure number within the bracket is the standard deviation of three (Sphagnum) or two (Eriophorum) replicate auto-chamber plots.

[c] RRMSE, relative root mean squared error, %.

Table 5 The systematic and unsystematic root mean squared errors ($RMSE_S$ and $RMSE_U$) between the modeled and observed daily net ecosystem exchanges (NEE) of CO_2 and CH_4 fluxes at the Palsa, Sphagnum, and Eriophorum sites.

Sites	NEE (mg C m^{-2} day^{-1})		CH_4 fluxes (mg C m^{-2} day^{-1})	
	$RMSE_S$	$RMSE_U$	$RMSE_S$	$RMSE_U$
Palsa	140	405		
Sphagnum	119	206	4.7	8.4
Eriophorum	298	545	16.7	46.6

Figure captions

Figure 1 Daily average air temperature, wind speed, precipitation, and solar radiation during 2002 to 2009. Data were recorded at the Abisko Scientific Research Station (ANS).

Figure 2 Simulated and observed seasonal dynamics of thaw depth at the Palsa (a to g), Sphagnum (h to n), and Eriophorum (o to u) sites during 2003 to 2009. The entire soil layer was thawed at the beginning of field observations (in mid June) at the Eriophorum site in 2007 (panel s).

Figure 3 Simulated and observed daily net ecosystem exchange (NEE) of CO_2 (mg C m^{-2} day^{-1}) at the Palsa (a to g), Sphagnum (h to n), and Eriophorum (o to u) sites during 2003 to 2009. The correlations between the simulated and observed daily NEE were significant for all cases ($P < 0.0001$, except for panel i, where $P < 0.001$). The observed data are the means of three (Palsa and Sphagnum) or two (Eriophorum) chamber replicates and standard deviations are not shown for reasons of clarity. Note that the vertical axis scales for NEE are different across the three sites.

Figure 4 Simulated (lines) and observed (dots) water table dynamics (a to g), daily CH_4 fluxes (mg C m^{-2} day^{-1}) at the Sphagnum (h to n) and Eriophorum (o to u) sites during 2003 to 2009. The correlations between the simulated and observed daily CH_4 fluxes were significant for all cases ($P < 0.0001$). The observed CH_4 fluxes are the means of three (Sphagnum) or two (Eriophorum) chamber replicates and standard deviations are not shown for reasons of clarity. Because of instrument problems (Bäckstrand et al., 2008), observed data were not used for model evaluation in 2006. Note that the vertical axis scales for CH_4 fluxes are different between the two sites.

Figure 5 Relationships between simulated CH_4 fluxes and average soil (0-50 cm)

temperatures as well as water table depths at the Sphagnum (a and b) and Eriophorum (c and d) sites. The results shown in the panels (a) and (c) are for periods with water table depth above -10 cm; the results shown in the panels (b) and (d) are for periods with average soil (0-50 cm) temperature > 2 °C. The relationships shown in panels (a), (b), and (c) were significant ($P < 0.0001$).

Figure 6 Simulated net ecosystem exchange (NEE) of CO_2, CH_4 fluxes, net carbon fluxes, and net emissions of greenhouse gases (GHG) at the Palsa, Sphagnum, and Eriophorum sites. The CH_4 fluxes from the dry Palsa site were assumed negligible (here 0), based on field observations. Data are means of annual total fluxes from 2003 to 2009. Vertical bars are standard deviations of annual total fluxes from 2003 to 2009 and indicate inter-annual variations of C gas fluxes.

1122 **Figure 1**

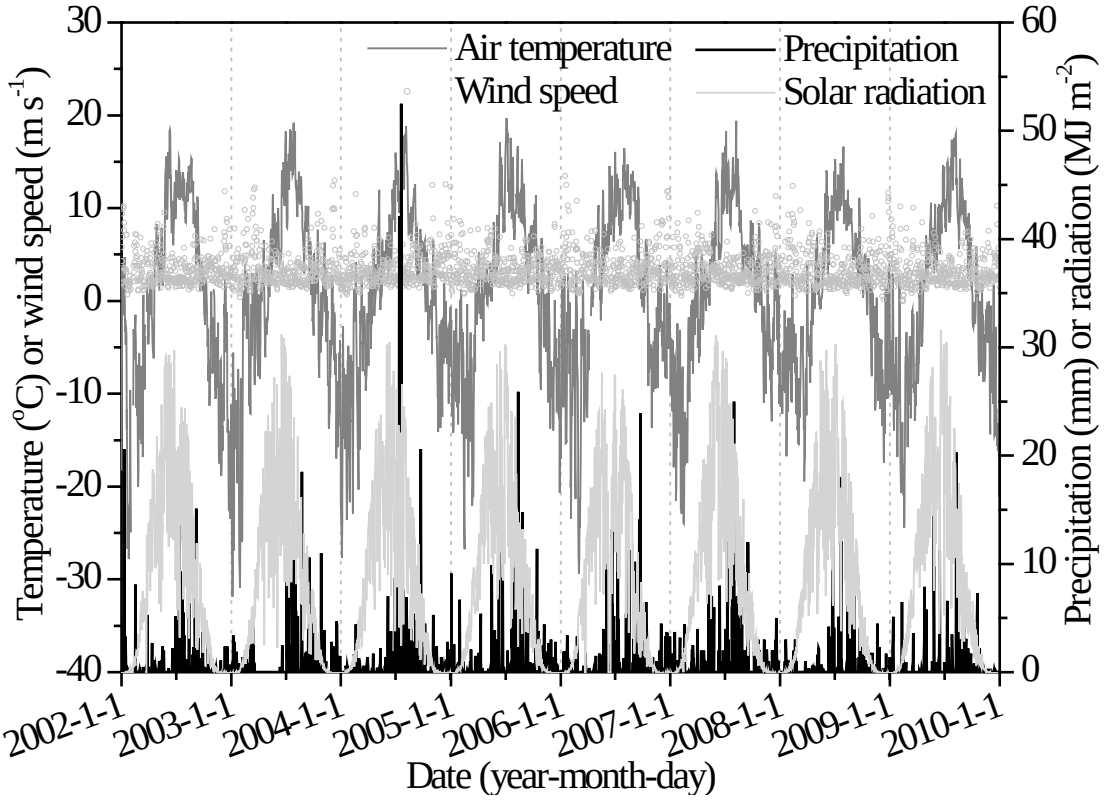

1123
1124

1125 **Figure 2**

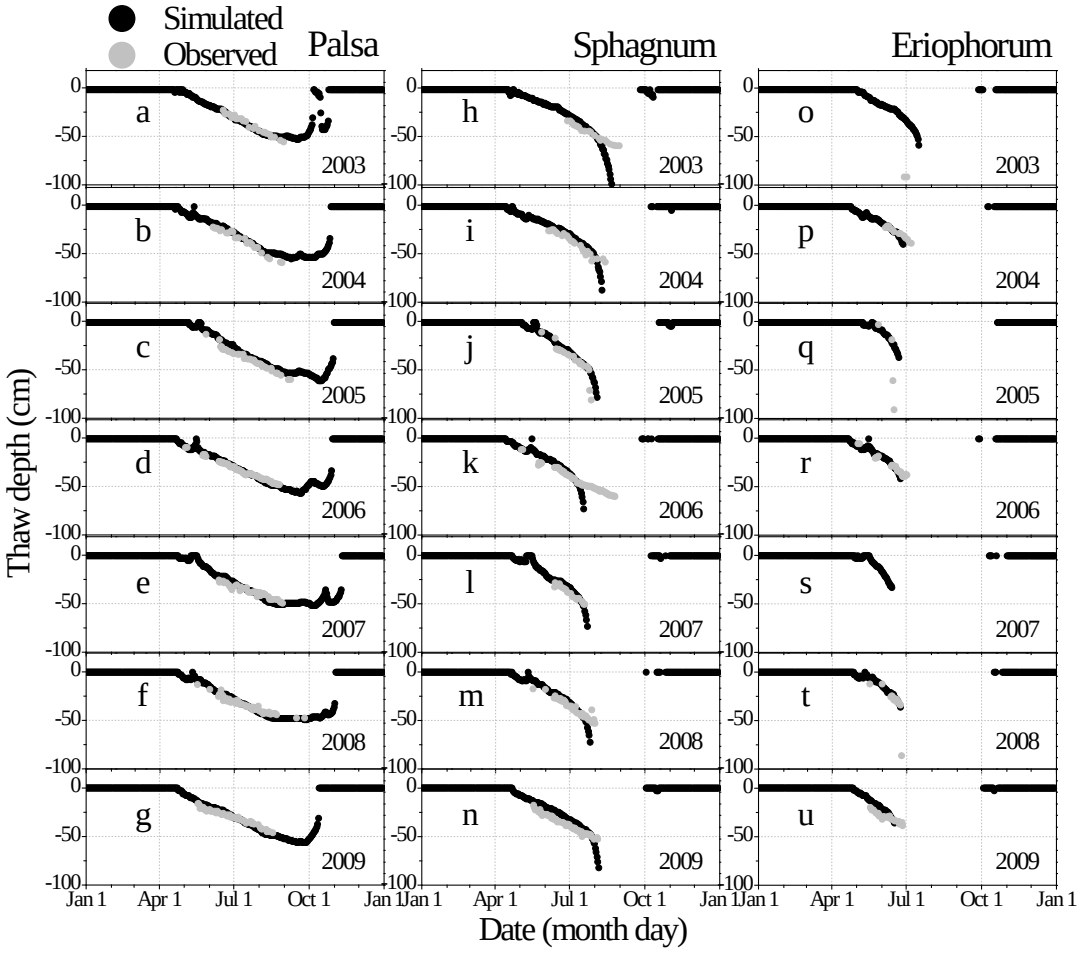

1126
1127

1128 **Figure 3**

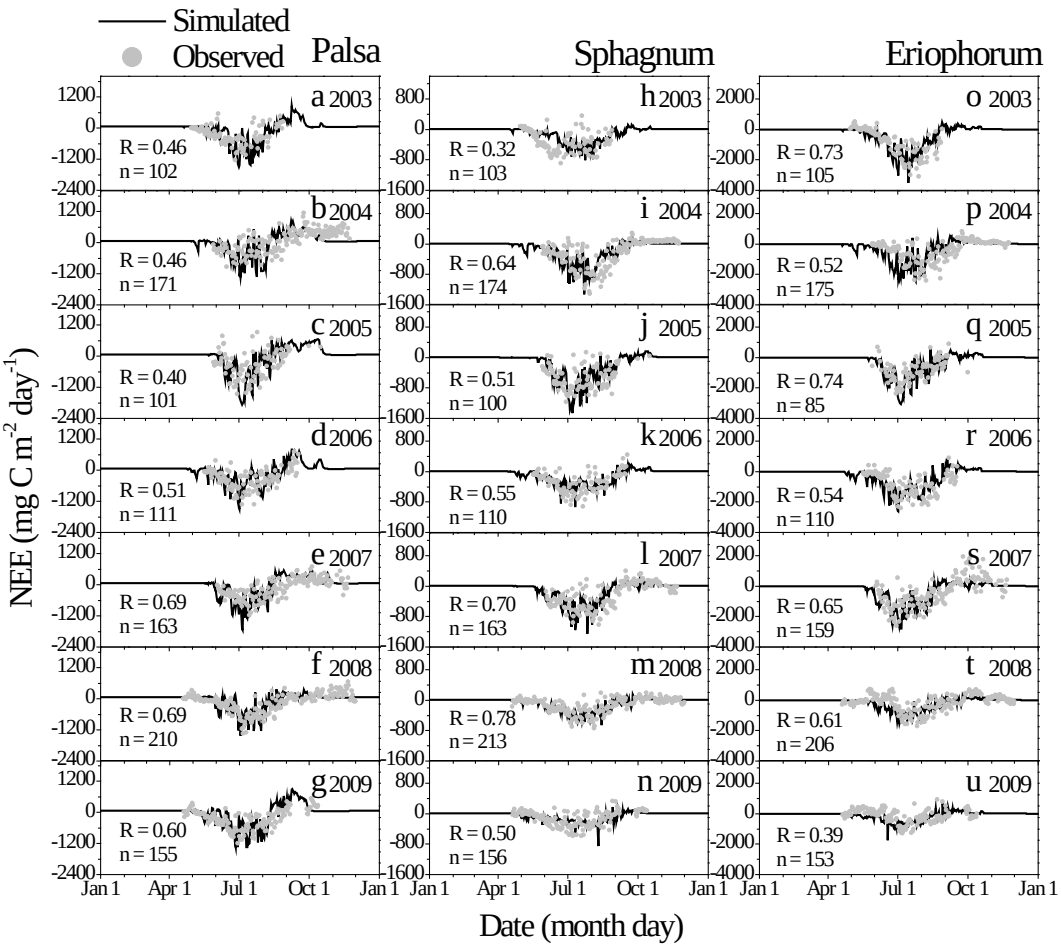

1129
1130

1131 **Figure 4**

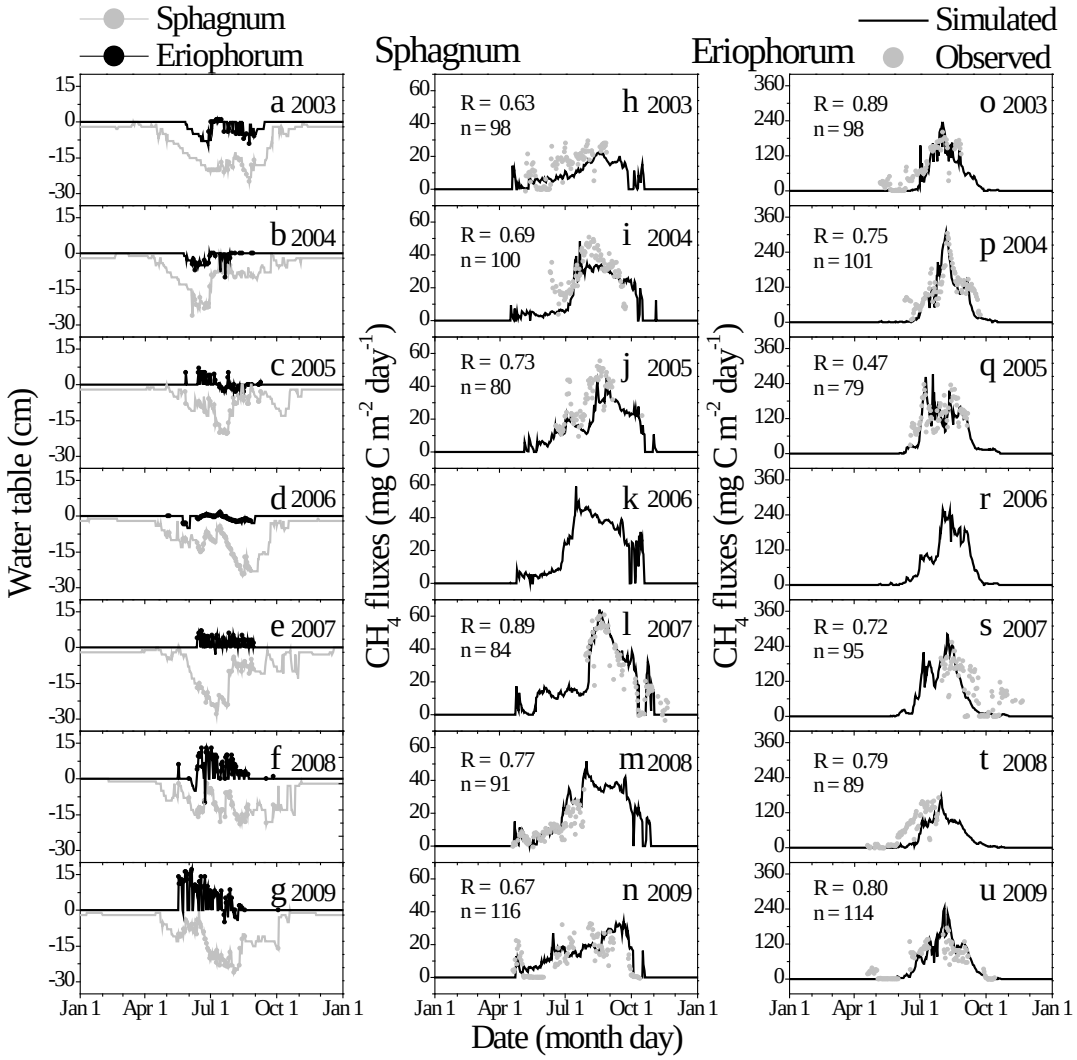

1132
1133

1134 **Figure 5**

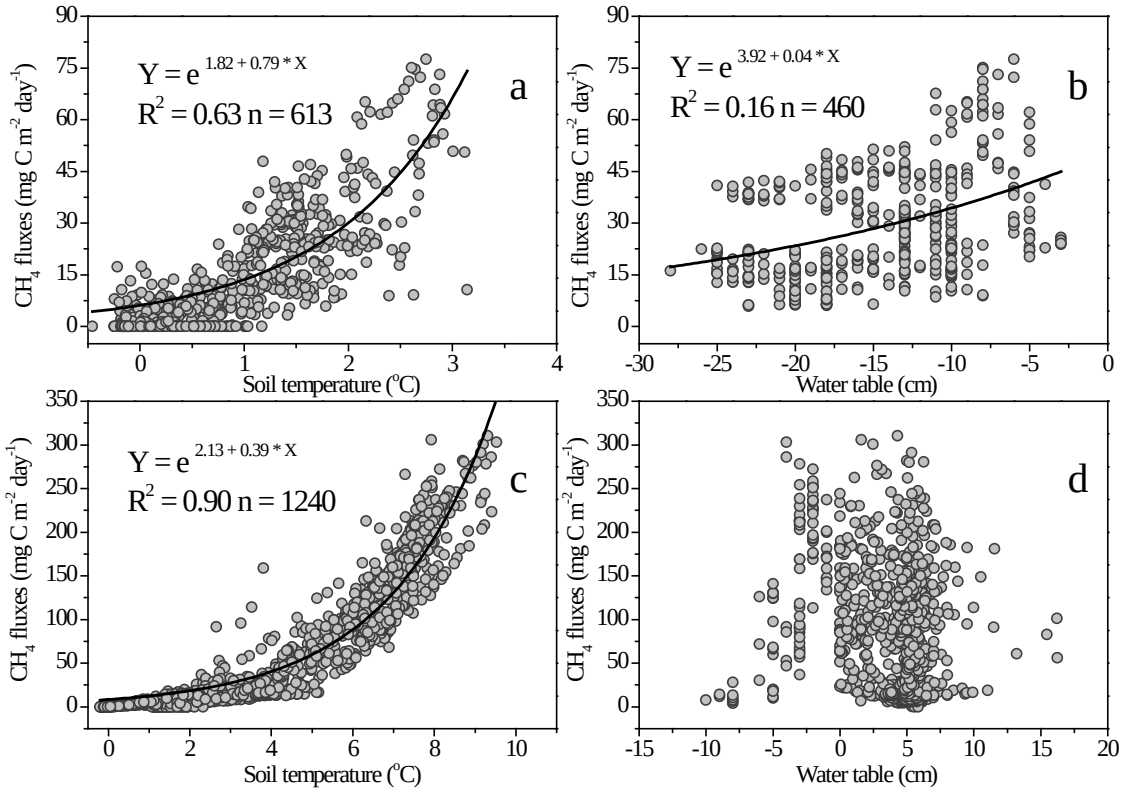

1135
1136

1137 **Figure 6**

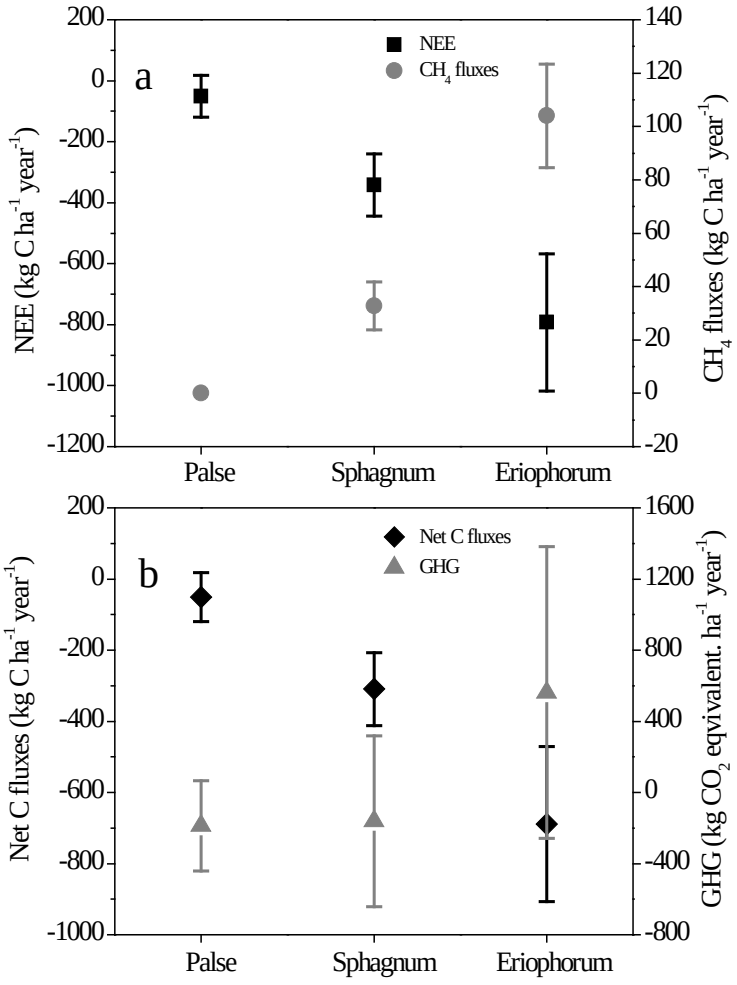

1138